Structural, Physical, and Biological Characteristics of RNA·DNA Binding Agent N8-Actinomycin D[†,‡]

Miho Shinomiya, Wenhua Chu, Robert G. Carlson, Robert F. Weaver, and Fusao Takusagawa*

Departments of Chemistry and Biochemistry, University of Kansas, Lawrence, Kansas 66045-0046

Received January 17, 1995; Revised Manuscript Received April 27, 1995[⊗]

ABSTRACT: The crystal structure of the self-complementary DNA octamer d(GAAGCTTC)$_2$ complexed with N8-actinomycin D (N8AMD) has been determined at 3.0 Å resolution (space group: $P3_121$; unit cell: a = 62.30, b = 62.30, c = 42.97 Å; R = 0.173 for 1845 reflections). The DNA structure was severely distorted by the N8AMD bound intercalatively into the middle dinucleotide, 5′-GC-3′. The two cyclic depsipeptides, which differ from each other in overall conformation, lie in the minor groove. The complex is further stabilized by forming base−peptide and chromophore−backbone hydrogen bonds. The complexes are stacked together to form a pseudocontinuous helix running through the crystals. The structure of d(GAAGCTTC)$_2$−actinomycin D (AMD) crystallized in the space group $C2$ [Kamitori S., & Takusagawa, F. (1992) *J. Mol. Biol. 225*, 445−456] was re-refined in order to compare it directly to the N8AMD complex structure. The asymmetrical binding mode of AMD has been confirmed on the basis of the two complex structures. The crystal structures of the N8AMD and AMD complexes bound to the same d(GAAGCTTC)$_2$ differed by a root-mean-square deviation on all atom positions of 1.77 Å, but most of the structural differences can be attributed to molecular packing in two different crystal forms, and not to structural differences induced by the interaction with the intercalating agents. However, the DNA binding and biological characteristics of N8AMD and AMD are quite different from each other. The DNA association constant of N8AMD is 33-fold less than that of AMD in an aqueous solution. N8AMD required a concentration >10.0 μM to inhibit RNA synthesis activity in HeLa cells by 50%, whereas AMD reached to the same inhibitory level at only 35 nM. The structure of the DNA-N8AMD complex suggested that substitution of the *N*-methyl-L-valine residue in the cyclic depsipeptide with a *N*-methyl-D-valine residue might increase the hydrophobic interaction with the minor groove of the DNA. Thus the DNA association constant and RNA synthesis inhibitory activities of 5,5′-*N*-methyl-D-valine AMD (D-MeVal-AMD) have also been determined. The DNA association constant of D-MeVal-AMD is more than 2-fold greater than that of AMD, and the RNA synthesis inhibitory activity is about 20-fold greater.

A group of compounds called intercalators bind intercalatively to DNA and interrupt RNA synthesis (transcription) and/or DNA synthesis (replication). Some intercalators have been used as anticancer drugs and others are carcinogens. There are several important questions to be answered in order to understand the biological activities of useful intercalators. Some of the questions are, how intercalators bind to DNA, how intercalators distort DNA structures, and how intercalators recognize their binding sequence. Three-dimensional structures of DNA−drug complexes are informative enough to answer these questions. For this reason, the crystal structures of the complexes between DNA (hexanucleotide) and anthracycline intercalators daunomycin (Quigley *et al.*, 1980; Wang *et al.*, 1987; Frederick *et al.*, 1990; Moore *et al.*, 1989; Nunn *et al.*, 1991), adriamycin (Frederick *et al.*, 1990; Lipscomb *et al.*, 1994), nogalamycin (Liaw *et al.*, 1989; Gao *et al.*, 1990; Williams *et al.*, 1990a; Egli *et al.*, 1991), and their derivatives (Williams *et al.*, 1990b; Cirilli *et al.*, 1992) have been determined at atomic resolution. The DNA complexes of bis-intercalators triostin A (Wang *et al.*, 1984, 1986; Ughetto *et al.*, 1985; Quigley *et al.*, 1986), echinomycin (Ughetto *et al.*, 1985), and ditercalinium (Gao *et al.*, 1991) have also been investigated by X-ray analyses. These structures showed many interesting DNA−drug interactions and geometrical features of the DNA−drug complexes at the atomic level. However, structural changes in DNA by the drug intercalation still could not be sufficiently observed, because one drug molecule intercalates at each end of the DNA fragment. Therefore, the crystal structure of a DNA−drug complex, in which a drug intercalates between the middle base pairs of a relatively long DNA fragment (hexamer or more), has been sought as a more practical model for biological systems.

Recently, we have determined the two crystal structures of the complexes between d(GAAGCTTC)$_2$ and AMD[1] crystallized in the space groups $C2$ (Kamitori & Takusagawa, 1992) and $F222$ (Kamitori & Takusagawa, 1994) in which AMD intercalated between the middle 5′-GC-3′ base pairs. These crystal structures of the complexes show how the drug

[†] This research was supported by NIH (AI28578), Marion Merrell Dow Foundation, J. R. and Inez W. Jay Research Foundation, and Kansas Health Foundation, Wichita, Kansas.

[‡] The atomic coordinates have been deposited with the Brookhaven Protein Data Bank (entry names: 209D).

* Author to whom correspondence should be addressed.

[⊗] Abstract published in *Advance ACS Abstracts,* June 15, 1995.

[1] Abbreviations used: AMD, actinomycin D; N8AMD, N8-actinomycin D; L-MeVal, *N*-methyl-L-valine; D-MeVal, *N*-methyl-D-valine; D-MeVal-AMD, 5,5′-*N*-methyl-D-valine-actinomycin D; rms, root-mean-square.

0006-2960/95/0434-8481$09.00/0

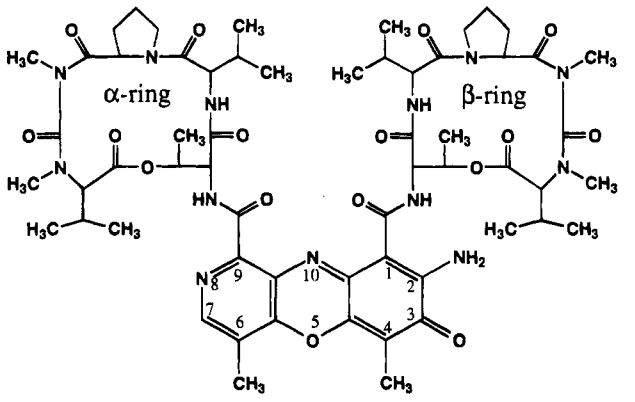

FIGURE 1: Molecular formula of N8-actinomycin D (N8AMD). The 8-position of the phenoxazone ring of actinomycin D (AMD) was replaced with a nitrogen atom.

interacts with DNA and explain why AMD cannot bind to RNA. The 2′-hydroxyl group of ribose would have unusually short contacts with the 2-amino group of the phenoxazone ring, if the deoxyribose of the guanosine is changed to ribose. Thus, it would be clearly impossible to replace the guanosine deoxyribose with ribose. However, if the C8-H of the phenoxazone ring is replaced by the strong hydrogen-bond acceptor N8 (Figure 1), the 2′-hydroxyl group of the guanosine ribose (RNA) will be able to make a hydrogen bond to N8. To test our hypothesis, we have actually synthesized N8AMD and examined the binding character of the agent to nucleic acids (Chu *et al.*, 1994a). This study indicates that N8AMD binds intercalatively not only to DNA·DNA double strands but also to RNA·DNA hybrids.

In vivo, HIV reverse transcriptase uses a lysine transfer RNA as a primer to make a minus strand DNA copy of the viral RNA as an RNA·DNA hybrid (Wain-Holson *et al.*, 1985). Besides having reverse transcriptase activity, the enzyme possesses an inherent RNase H activity that specifically degrades the RNA of the RNA·DNA hybrid (Swanstorm *et al.*, 1981; Resnick *et al.*, 1984; Omer & Faras, 1982; Gerard, 1981; Champoux *et al.*, 1984; Verma, 1977). Therefore, in theory, inhibition of this process would suppress viral replication. Thus, we are looking for agents that bind only to the RNA·DNA hybrid, but neither to double-stranded DNA nor to RNA. Such agents would specifically inhibit the RNase H activity of reverse transcriptase and, therefore, suppress viral replication. In order to develop such agents, one must accumulate structural, physical, and biological data. Here we report the crystal structure of the d(GAAGCTTC)$_2$−N8AMD complex and the physical and biological characteristics of N8AMD in comparison with AMD.

EXPERIMENTAL PROCEDURES

Crystallization of N8AMD Complex. Several self-complementary octanucleotides, d(ZYXGCX′Y′Z′), which contain the AMD binding sequence, 5′-XGCX′-3′ (X ≠ G and X′ ≠ C) (Scamrov & Beabealashvilli, 1983), in the middle, were synthesized by using a fully automated DNA synthesizer (Cruachem P250). The residues X and Y in the sites adjacent to the intercalation site were A or T, and the edge residue Z was C or G to prevent opening of the double helix. Reverse-phase HPLC was used to obtain pure oligonucleotides. N8AMD was synthesized totally in our laboratory (Chu *et al.*, 1994a). The relatively large complex crystals were grown from the crystallization mixture of d(GAAGCTTC)$_2$−N8AMD. A typical crystallization mixture contained 2.0 mM oligonucleotide, 10 mM $MgCl_2$, 20 mM cacodylate (pH 7.0), 2 mM spermine tetrachloride, and 1.5 mM N8AMD in 7.5% (v/v) 2-methyl-2,4-pentanediol (MPD). Hanging drops (20 μL) of the mixture were equilibrated with 15% MPD in an incubator at 26 °C by vapor diffusion. Orange-red crystals appeared after 2 weeks. The crystal used for measurement of the X-ray diffraction data was dissolved in 1.0 mL water, and the ratio of DNA to drug was determined by spectroscopic methods. The ratio of absorbances at 260 and 426 nm was 8.0, which agreed well with 7.3 obtained from the 1:1 double-stranded DNA and drug in mixed solution (ratios of 1:2 and 2:1 give 4.0 and 11.3, respectively). Therefore, the crystal used for X-ray data measurement should contain equimolar quantities of the double-stranded DNA and the drug.

Structure Determination of the N8AMD Complex. A hexagonal plate shaped crystal (0.5 × 0.5 × 0.15 mm) of the DNA−N8AMD complex was mounted into a glass capillary with mother liquor. The data were measured on a locally modified DIP100S imaging plate X-ray diffractometer (MAC Science) at room temperature using a graphite-monochromated Cu Kα radiation (λ = 1.5418 Å). The still photographs indicated that the crystal diffracted to 3.0 Å resolution in the *a* and *b* axes directions and to 3.2 Å resolution in others. The unit cell dimension was determined from the still photographs by software developed locally and was further refined, along with the crystal orientation, by the ELMS software associated with DIP100S (Tanaka *et al.*, 1992). It is noted that the *a* and *b* axes dimension is a multiple of 2 × (8 + 1) × 3.4 ≈ 61.4 Å, suggesting that the complex is an octamer duplex with one N8AMD intercalated in it, and the complexes are stacked on each other along the *a* and *b* axes so as to form a pseudocontinuous helix. Intensity data were measured to a resolution of 3.0 Å. The diffraction data indicated that the crystal belonged to the trigonal system with the space group $P3_121$ or $P3_221$. Integrated intensities of the reflections were scaled and reduced with locally developed programs (Takusagawa, 1992). A total of 1845 independent reflections in 7−3 Å resolution were obtained and used in subsequent structure determination and refinement.

The Patterson map of the DNA−N8AMD complex calculated with 7−3 Å resolution data shows clearly the planar base stacking direction (helical axis direction), which is along the *a* and *b* axes direction. This feature of the map is consistent with the unit cell dimensions described above. This characteristic feature of the Patterson map as well as the crystallographic information (space group and unit cell dimension) suggest, that the complexes in the crystal lie on the crystallographic 2-fold screw axes along the [1 0 0], [0 1 0], and [1 1 0] directions to form a pseudocontinuous helix. This interpretation of the Patterson map was confirmed by the molecular replacement method using the crystal structures of DNA−AMD complexes (Kamitori & Takusagawa, 1992, 1994). The asymmetrical model [*C*2 crystal form taken from Kamitori and Takusagawa (1992)] and the symmetrical model [*F*222 crystal form taken from Kamitori and Takusagawa (1994)] were utilized for searching. Each model was initially positioned so that the helical axis coincided with the 2-fold screw axis along the *a* axis. The model was rotated around the helical axis by 5° steps and translated

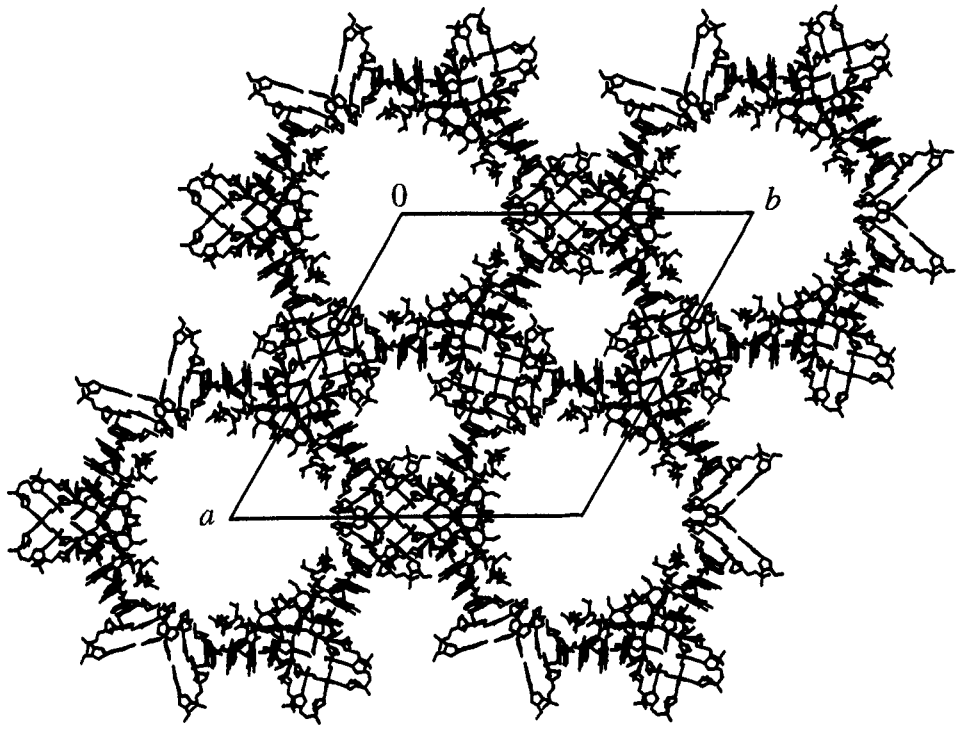

FIGURE 2: Molecular packing diagram viewed along the *c*-axis showing large solvent channels in the crystal structure. The pseudocontinuous helices run along the [1 0 0], [0 1 0], and [1 1 0] directions in the unit cell.

along the *a* axis by 0.5 Å steps, and it was refined at each stepped position by a rigid-body least-squares method (Takusagawa, 1982), using 5−3 Å resolution data (497 reflections above 5σ). Two possible space groups, $P3_121$ and $P3_221$, were examined. This procedure provided seven local minima of the *R* factors. These seven structures were then refined by the program X-PLOR (Brünger, 1993), using 7−3 Å resolution data (1093 reflections above 3σ). Although the *R* factors of all models went to around 0.32, most of the refined complex structures were not acceptable in geometrical terms, e.g., they had no base-pairing and they had short intermolecular contacts. The structure derived from the asymmetrical model (*C*2 crystal form) with the space group $P3_121$ gave the lowest *R* factor as well as the best geometrical features. Therefore, this structure was further refined using the method of simulated annealing with the program X-PLOR (Brünger, 1993). The progress of refinement was followed by inspection of electron density maps on a graphics workstation using FRODO (Jones, 1985). Since the bases formed Watson−Crick base pairs, those base pair hydrogen bonds are constrained in the refinement. Although the V_M value defined by Matthews (1968) was relatively high (3.9 Å/Da) and the molecular packing showed a large solvent channel along the *c* axis at each corner of the unit cell (Figure 2), the difference maps did not show any additional N8AMD molecule and/or DNA in the channel. Water molecules were picked up in the ($F_o - F_c$) and ($2F_o - F_c$) maps using 2.8 Å separation criteria and introduced gradually in the refinement. Refinement of the isotropic temperature factor for individual atoms was carried out by the individual *B* factor refinement procedure of X-PLOR using bond (1−2) and angle (1−3) restraints. The anisotropic zone scaling procedure was applied in order to correct the absorption effect and/or unknown systematic error in the observed structure factors. The current structure contains one complex and 105 water molecules, and the *R* factor is 17.3% with all 1845 reflections at 7.0−3.0 Å resolution.

The final model was replaced with the symmetrical model [*F*222 crystal form taken from Kamitori and Takusagawa (1994)], and the model was varied first with the method of simulated annealing and then with the positional refinement procedure of the program X-PLOR (Brünger, 1993), in order to examine whether the initial symmetrical model converts to the asymmetrical final model. This procedure gave the same structure derived from the initial asymmetric model described above, indicating that the final model does not contain the bias of the initial search model.

Although the crystallographic *R* factor is relatively low, the structure determined at 3.0 Å resolution should be proven by another method besides the *R* factor. Four omit difference maps were calculated in order to confirm the structure analysis, as has been applied in the structure analysis of the *C*2 crystal form of the AMD complex (Kamitori & Takusagawa, 1992). Those are (1) β-ring of N8AMD, (2) chromophore of N8AMD, (3) $G_4 \equiv C_{13}$ base pair, and (4) phosphate groups in the intercalation site. The omit difference map of the β-ring (Figure 3A) shows significant electron density along the backbone of the cyclic depsipeptide. The electron density of the chromophore (Figure 3B) and the base pair (Figure 3C) are clearly distinguishable from each other. The chromophore has a large disk-shaped electron density whereas the base pair has a separate electron density for each base. The significant electron density of the phosphate sites (Figure 3D) indicates that the N8AMD does intercalate in the middle of the sequence, rather than between the double helices. These four omit difference maps demonstrate that the crystal structure of the complex has been correctly determined at 3.0 Å resolution. The crystallographic data are listed in Table 1.

Precise conformational details, accurate hydrogen-bond geometry, contact distances, and features such as the positions of water molecules—all of which may be significant

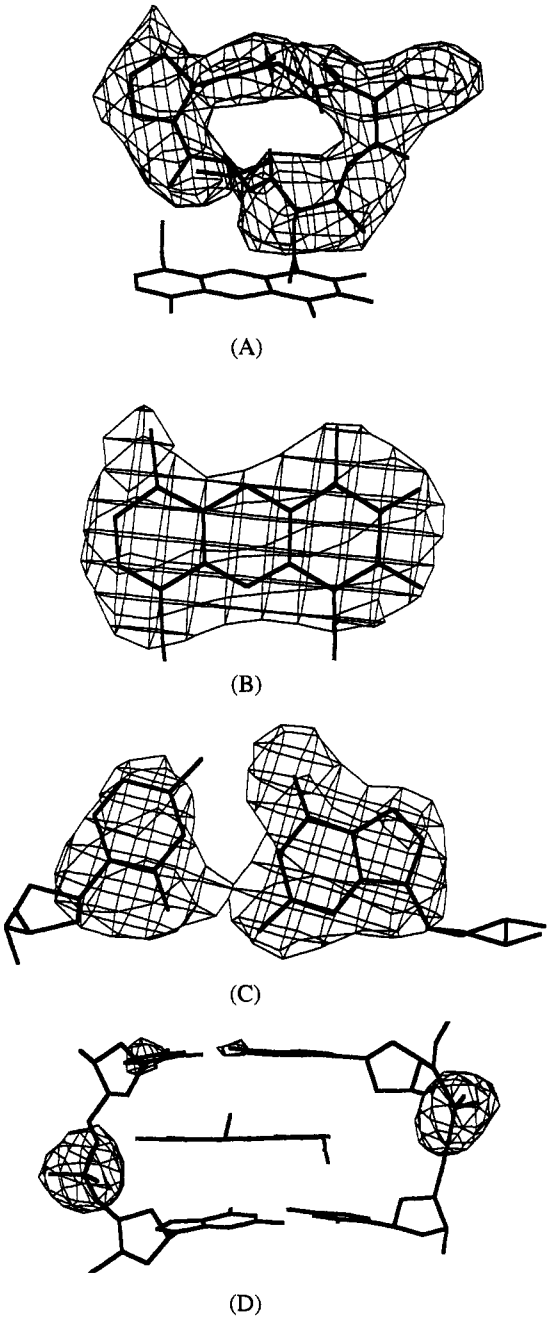

FIGURE 3: Omit difference maps. The contour levels are at 3.0σ except for panel A, which is 2.0σ. The omit difference maps were calculated with the amplitudes of ($F_o - F_c$) and phase angles (α_c), where F_o is an observed structure factor, and F_c and α_c are a structure factor and phase angle, respectively, obtained after 30 cycles of positional refinement by X-PLOR using the partially omitted final structure. The omitted portions are (A) β-ring (five amino acid residues), (B) chromophore, (C) G4≡C13 base pair, and (D) two phosphate groups (PO_4) in the intercalation site.

for complete understanding of DNA−drug interaction—will be visible only at higher resolution. The structure determined at around 3.0 Å resolution, however, provides relatively accurate positions and orientations of rigid groups, such as bases and base pairs. The overall conformations of the DNA backbone and cyclic peptide rings are also visible at this resolution. Intermolecular interactions, mainly hydrogen bonds, are distinguishable. Thus, we believe our present structure to be sufficiently well determined to address many key questions regarding DNA−N8AMD interactions.

Table 1: Crystallographic and Refinement Data

molecular form	d(GAAGCTTC)$_2$−N8AMD ($C_{78}H_{92}N_{30}P_7O_{46}$)$_2$−$C_{61}H_{85}N_{13}O_{16}$
formula weight	6057
space group	$P3_121$
unit cell dimensions	
a (Å)	62.30
b (Å)	62.30
c (Å)	42.97
no. formula in asymmetric unit	1
crystal size (mm)	0.5 × 0.5 × 0.15
resolution (Å)	7.0−3.0
no. reflections measured	21449
no. unique reflections	1845 (95% complete)
R_{sym}	0.072
no. water molecules	105
R-factor (all data)	0.173
rms deviations from ideal stereochemistry	
bond distances (Å)	0.018
bond angles (deg)	4.1
dihedral angle(deg)	25.5

Refinement of the d(GAAGCTTC)$_2$−AMD Complex Crystallized in the C2 Crystal Form. The complex of d(GAAGCTTC)$_2$−AMD has been crystallized into two crystal forms, *C*2 and *F*222 (Kamitori & Takusagawa, 1992, 1994). In the *F*222 crystal form, two independent complexes are located on the crystallographic 2-fold axes, indicating that the complex structures in this crystal form are disordered. On the other hand, the crystal structure of the d(GAAGCTTC)$_2$−AMD complex crystallized in the *C*2 crystal form contains one complex in the crystallographic asymmetric unit as seen in the N8AMD complex. However, the crystal structure of the *C*2 crystal form was refined slightly differently from the N8AMD structure. Thus the structure of the AMD complex was re-refined with the same procedure applied to the structure refinement of the N8AMD complex, in order to evaluate the structure of the N8AMD complex in comparison with the similar AMD complex. Watson−Crick base pair hydrogen bonds were all constrained, and the individual temperature factors were refined by the restrained procedure using bond (1−2) and angle (1−3) criteria. Although all the data (1360 reflections) in the 7.0−3.0 Å resolution range were used for refinement of the structure and the geometry and temperature factors were constrained, the *R* factor (0.190) is as low as the *R* factor (0.187) of the previous refinement with 1.5σ cut off data (1055 reflections) and no hydrogen-bond constraint. The rms deviations from the ideal geometry are much improved in comparison with the previous refinement and are listed in Table 2. Two water molecules located between the drug and DNA were eliminated. The new coordinates have been deposited with Brookhaven Protein Data Bank (entry names: 2D55).

UV/Vis Spectrum Measurements. UV/Vis absorption spectra were measured on a JASCO V-560 double beam spectrometer. A stock solution (20 μM) of d(GAAGCTTC)$_2$ was prepared with binding buffer [50 mM Tris-HCl (pH 7.5), 10 mM $MgCl_2$, and 10.0 mM KCl)]. All binding experiments were carried out in the same buffer. The concentration of the DNA (single strand) was determined from the absorbance at 260 nm using the extinction coefficient 72.5 × 10^3 M^{-1} cm^{-1} (Cantor & Warshaw, 1970). The concentrations of N8AMD, AMD, and D-MeVal-AMD solutions were determined from the absorbances at 426, 440, and 440

Table 2: Refinement Parameters of the d(GAAGCTTC)$_2$−AMD Complex

molecular form	d(GAAGCTTC)$_2$−AMD ($C_{78}H_{92}N_{30}P_7O_{46})_2$−$C_{62}H_{86}N_{12}O_{16}$
formula weight	6056
space group	C2
resolution (Å)	7.0−3.0
no. unique reflections	1360 (100% complete)
no. water molecules	105
R factor (all data)	0.190
rms deviations from ideal stereochemistry	
bond distances (Å)	0.019
bond angles (deg)	4.8
dihedral angle(deg)	25.7

nm, respectively, using an extinction coefficient of 2.45 × 10^4 M^{-1} cm^{-1} (Chen, 1988).

The absorption spectra of drug during titration with d(GAAGCTTC)$_2$ were obtained in order to examine the binding characteristics of drug to the oligonucleotide. After the absorbance of 1.0 mL of drug solution (~1.0 μM) in binding buffer was measured from 600 to 350 nm for AMD and D-MeVal-AMD and from 575 to 325 nm for N8AMD at 4 °C, a small aliquot of a known concentration of the DNA solution was placed in the sample cuvette, and spectra were measured 5 min later. This procedure was repeated six times so that six spectra were measured at six different DNA concentrations. The absorbances of visible spectra were read at 1 nm intervals. Dilution factors were applied to all spectra. The association constants of N8AMD, AMD, and D-MeVal-AMD were calculated on the basis of the spectra using the method developed in our laboratory (Chu *et al.*, 1994b).

RNA Polymerase Inhibition. Human (HeLa) cells were cultured at 37 °C in a 1:1 mixture of DME and Ham's F-12 medium, supplemented with penicillin and streptomycin and 5% fetal bovine serum, in an atmosphere of 5.5% CO_2, using a total sodium bicarbonate concentration of 2.3 g/L. The cells were incubated in duplicate cultures with various concentrations of the drugs for 30 min. Then 10 μCi of [^{3}H]-uridine was added to label the RNA synthesized during a 30 min incubation at 37 °C. The labeled RNA was isolated by the rapid procedure of Chomczynski and Sacchi (1987). This involves homogenization of the cells in the presence of guanidine thiocyanate to inhibit RNases, acid phenol/chloroform extraction to remove protein and DNA, concentration by isopropanol precipitation, and dissolving the RNA in TE [10 mM Tris-HCl (pH 8.0), 1 mM EDTA]. The label incorporated into RNA was determined by liquid scintillation counting.

RESULTS AND DISCUSSION

Overall Structure of N8AMD Complex. As schematically illustrated in Figure 4, the chromophore of the N8AMD molecule intercalates via the minor groove into the middle (5′-GC-3′) of the oligonucleotide, and the two cyclic depsipeptides lie on both sides of the minor groove. The DNA numbering and standard convention are illustrated in Figure 4. The DNA helix is unwound by about 30° at the intercalation site, G4-C5, and the G4≡C13 and C5≡G12 base pairs are opened up to 7.1 Å. The two cyclic depsipeptide rings cover four base pairs (A3=T14, G4≡C13, C5≡G12, and T6=A11) of the DNA (Figure 5). N8AMD

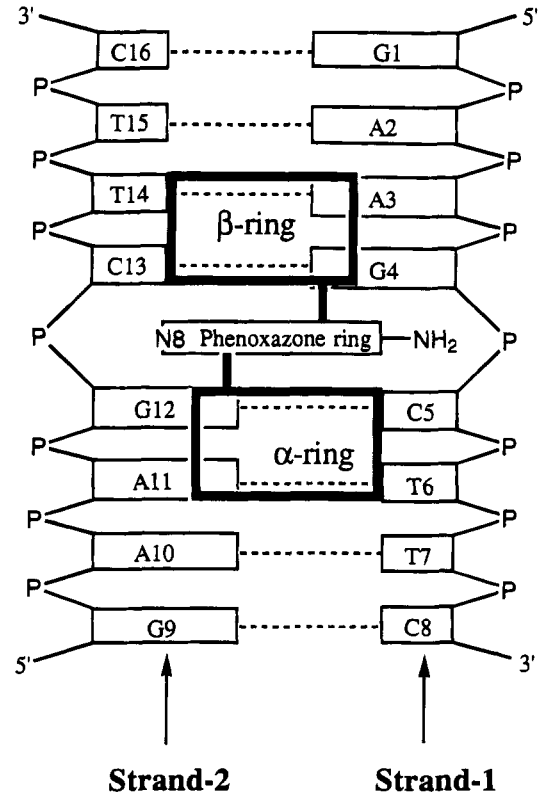

FIGURE 4: Schematic diagram of the d(GAAGCTTC)$_2$−N8AMD as observed in the crystal structure. The DNA strand numbered G1-A2-A3-G4-C5-T6-T7-C8, which is located on the side of the amino group (NH_2) of the chromophore, is named strand-1; the other DNA strand numbered G9-A10-A11-G12-C13-T14-T15-C16, which is located on the side of the N8 atom, is named strand-2. The cyclic depsipeptide attached at C9 of the chromophore is called the α-ring, and the other cyclic depsipeptide, which is attached at C1 and is near the amino group (NH_2), is called the β-ring (Meienhofer & Atherton, 1977).

is tightly connected to the DNA at the middle portion of the molecule by forming four threonine−guanine hydrogen bonds and an additional hydrogen bond between the N2 amino group of phenoxazone and the DNA backbone. The four threonine−guanine hydrogen bonds appear to recognize the DNA sequence 5′-GC-3′ as pointed out by Sobell and Jain (1972). These essential hydrogen bonds are covered by cyclic depsipeptides, which are constructed with mainly hydrophobic amino acid residues. These binding features of N8AMD are the same as those found in the AMD complexes (Kamitori & Takusagawa, 1992, 1994). The complexes are stacked together to form a pseudocontinuous helix running through the crystals. Stereoscopic views of the pseudocontinuous helices of N8AMD and AMD are illustrated in Figures 5 and 6.

As predicted by the molecular mechanics calculation (Chu *et al.*, 1994a), the substituted N8 atom in the phenoxazone ring does not participate in any hydrogen bonds to DNA. Although no distinguished water molecules were found within hydrogen bonding distance, a few disordered water molecules, which are difficult to identify in the 3.0 Å resolution map, should coordinate to the N8 atom by hydrogen bonds. The backbone of the DNA strand-2, which is located on the same side as the N8 atom, lies far away from the N8 atom. In particular, the phosphate group between the G12 and C13 residues is located as if the negatively charged PO_4 group is pushed far away by the

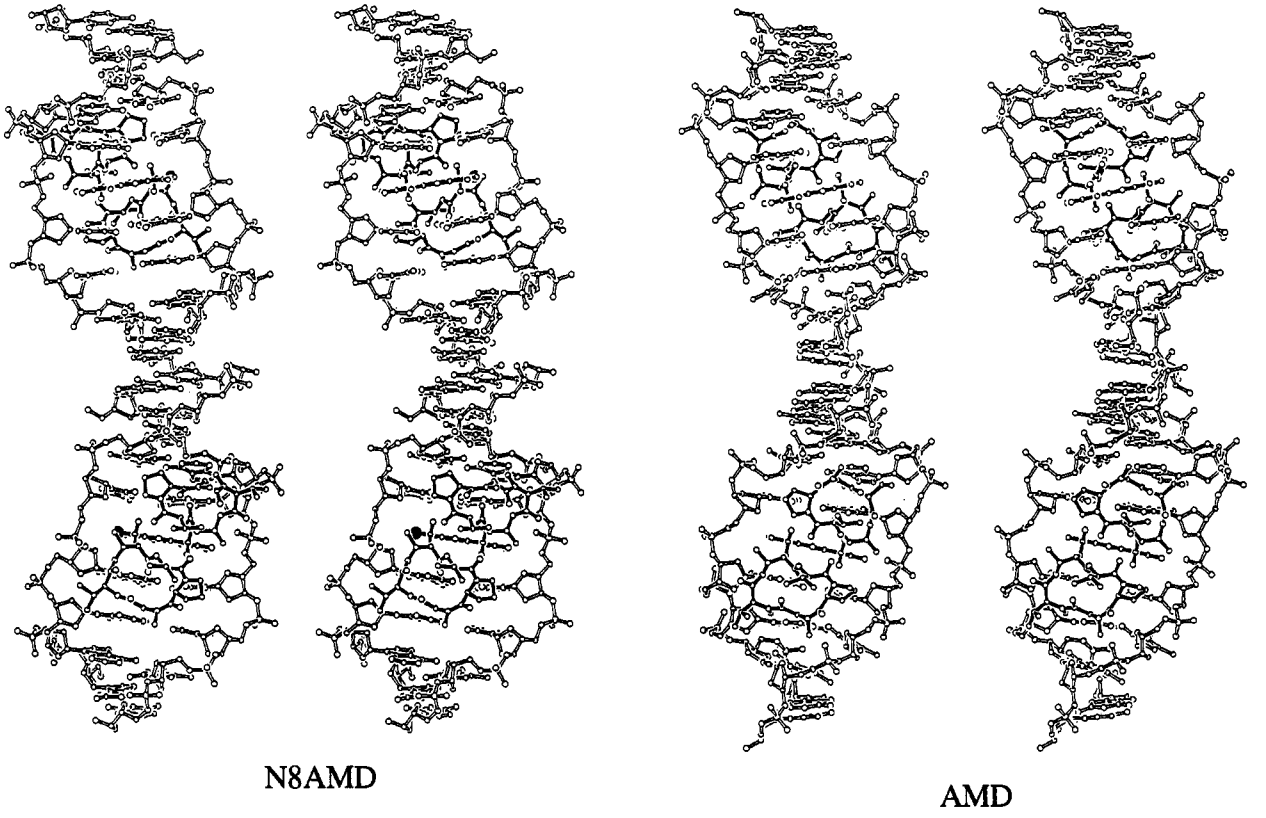

FIGURE 5: Stereodrawings of the pseudocontinuous helical structures of the d(GAAGCTTC)$_2$−N8AMD complex (left) and the re-refined d(GAAGCTTC)$_2$−AMD complex (right). The top and bottom portions of the helix represent the views of the major and minor grooves, respectively. The α-ring and β-ring of the cyclic depsipeptides are below and above the phenoxazone ring, respectively. The N8AMD and AMD molecules are illustrated with solid bonds while the DNA octamer has open bonds. The N8 atoms in the N8AMD complex are indicated by large filled circles.

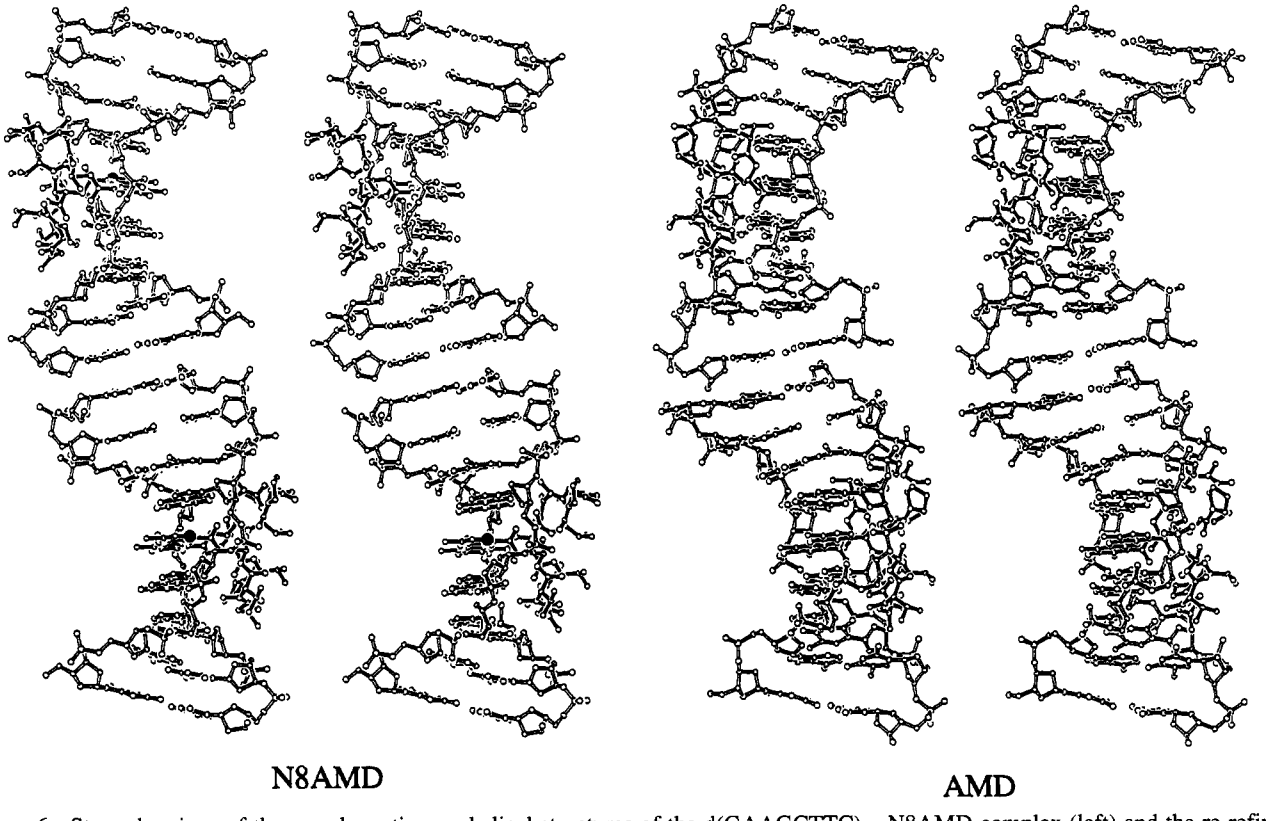

FIGURE 6: Stereodrawings of the pseudocontinuous helical structures of the d(GAAGCTTC)$_2$−N8AMD complex (left) and the re-refined d(GAAGCTTC)$_2$−AMD complex (right). The top and bottom portions of the helix represent the DNA strand-1 and strand-2 on the same side as the amino group (N2) and the N8 atom of the phenoxazone ring, respectively. The α-ring and β-ring of the cyclic depsipeptides are below and above the phenoxazone ring, respectively. The N8AMD and AMD molecules are illustrated with solid bonds, while the DNA octamer has open bonds. The N8 atoms in the N8AMD complex are indicated by large filled circles.

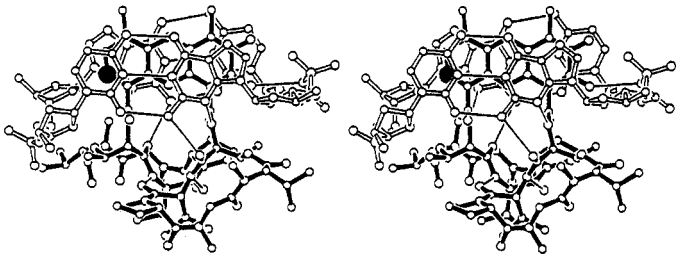

N8AMD

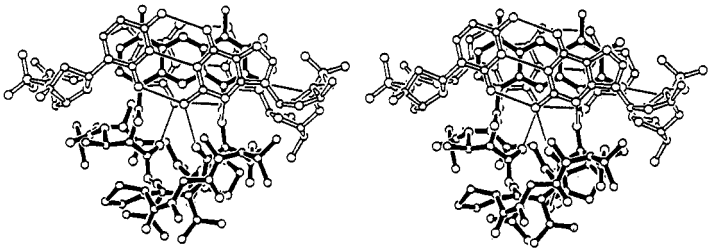

AMD
(A)

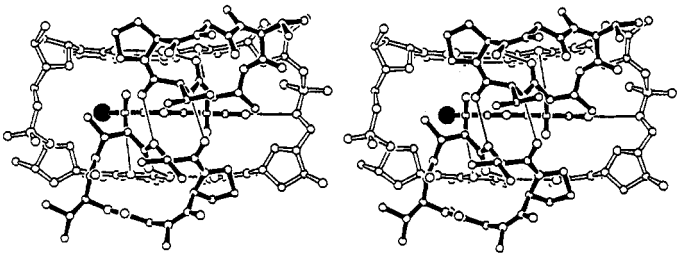

N8AMD

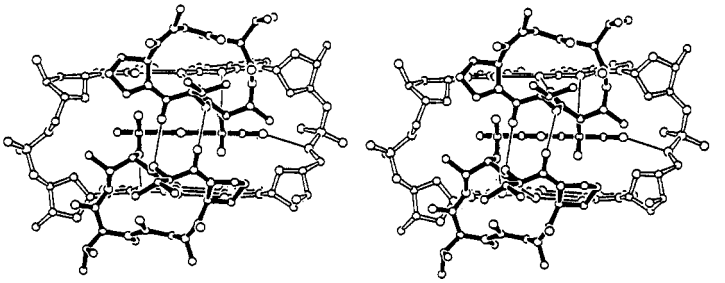

AMD
(B)

FIGURE 7: Hydrogen bonding scheme at the binding site. (A) Projection of the complex onto the plane of the chromophore. The G4≡C13 and C5≡G12 base pairs are above and below the phenoxazone ring, respectively. The drugs and DNA are drawn with solid and open bonds, respectively. The hydrogen bonds are indicated with thin lines. (B) Projection viewed down the O5−N10 vector of N8AMD or AMD molecule.

negatively charged N8 atom, whereas the backbone of the other DNA strand (strand-1) is bent to form a hydrogen bond with the amino group (N2) attached to the phenoxazone ring (Figures 6 and 7).

The root-mean-square (rms) deviations between the structures of the N8AMD and AMD complexes were calculated in order to examine how the complex structure was changed by the substitution of the N8 atom (Table 3). The rms

Table 3: RMS Deviations (Å) between N8AMD and AMD Complexes

portion	rms deviation (Å)
complex	1.77
double strand DNA	1.77
strand-1 (N2-amino group side)	1.82
strand-2 (N8-atom side)	1.61
drug	1.14
phenoxazone ring	0.12
depsipeptide ring (α-ring)	0.92
depsipeptide ring (β-ring)	0.76

deviation between the two DNA structures is larger than the rms deviation between the N8AMD and AMD molecules, suggesting that substituting the C-H with N at the 8-position of the phenoxazone ring does not significantly change the N8AMD structure from the AMD structure. The DNA strand-1 has a larger rms deviation than that of the DNA strand-2 located on the same side as the N8 atom, indicating that the N8 substitution has little effect on the complex structure. Thus, the structural differences between the N8AMD and AMD complexes are mainly due to the differences in molecular packing. As shown in Figure 2, the continuous pseudohelices in the N8AMD complex structure run along the [1 0 0], [0 1 0], and [1 1 0] directions in the unit cell, and thus those helices must cross over three times within the 42.97 Å space of the *c*-axis length. Since the sections of the pseudoconnections between the two complexes are the flattest through the pseudocontinuous DNA helices (Figure 6), the major grooves of the pseudocontinuous DNAs face each other as they cross near the section of the pseudoconnection region in order to avoid short contacts. Such a molecular packing probably requires an additional small bend and/or unwinding of the DNA helix, which slightly increases the rms deviations in the DNA structure. On the other hand, there is no such tight packing between the DNAs in the AMD complex structure, although the depsipeptides of AMD have hydrophobic interactions with those of the neighboring AMD molecule.

In the complexed DNA structure, the base pair rise at the intercalation site is approximately twice that at other sites (Table 4). The mean base pair rise excluding the intercalation site is 3.4 Å in both N8AMD and AMD complex structures, which is in good agreement with the value observed in the canonical B-form DNA (Dickerson, 1992). The helices are greatly unwound at the intercalation sites. The helix twist angle at the intercalation sites is 5°, indicating a larger unwinding, similar to that with AMD, has taken place (Table 4). It is impossible to determine the helical axes of severely distorted DNAs by using standard methods (Dickerson, 1989). The helical axes calculated by the top and bottom four base pairs indicate the DNAs are kinked at the intercalation site by 26° for N8AMD and 19° for AMD complexes. However, since DNA structures are severely distorted by intercalation of drugs and molecular packing, the two helical axes determined from the structures contain relatively large ambiguity. Thus, it is difficult to conclude from these data whether DNAs are kinked at the intercalation sites. Similarly, it is impossible to conclude whether the DNAs adopt the A- or B-conformation.

Binding Site Geometry in the N8AMD Complex. The geometries of the intercalation sites are shown in Figure 7. The binding modes of N8AMD are identical to those of AMD. The phenoxazone ring intercalates between the G4≡C13 and C5≡G12 base pairs of the DNA via the minor groove. The two methyl groups (C15 and C16) attached to the phenoxazone ring pass between the base pairs during binding and protrude out of the major groove of the DNA on the opposite side; they appear to play the role of anchor to prevent easy separation of N8AMD from the DNA. N2−H(G)···O(Thr) and N−H(Thr)···N3(G) hydrogen bonds, which recognize the intercalation site, 5′-GC-3′, are observed in all DNA−AMD complexes. The methyl groups of threonine and *N*-methyl groups of methylvaline residues in the cyclic depsipeptides are pointed toward the DNA minor groove as if those groups cover the essential threonine−guanine hydrogen bonds. Two cyclic depsipeptides are connected through two interring hydrogen bonds between the amide groups and carbonyl oxygen atoms of the D-valine residues, which appear to reduce the mobility of the rings. In the view described above, both N8AMD and AMD biding sites have a 2-fold symmetry. However, as shown in Figures 5 and 7, the conformations of the two cyclic depsipeptides are significantly different from each other. The α-ring fits well into the minor groove of DNA, whereas the β-ring appears to be forced out of the DNA minor groove. These different interactions of the two cyclic depsipeptides with the DNA minor groove break the 2-fold symmetry of the binding site geometry. Although this asymmetry feature was found previously in the structure of the DNA−AMD complex (Kamitori & Takusagawa, 1992), no speculation on the reason was given since there was no other similar structure at that time. Now the same trend is observed in the N8AMD complex, suggesting a common feature of the AMD binding mode.

In addition to the base−peptide hydrogen bonds described above, the amino group (N2) attached to the phenoxazone ring is involved in hydrogen bonding to O5′ of the cytosine C5 residue. In general, a DNA helix is unwound by

Table 4: Helix Twist Angles and Base Pair Rise Parameters[a]

	helix twist angles (deg)							
	G1-A2	A2-A3	A3-G4	G4-C5	C5-T6	T6-T7	T7-C8	mean[b]
N8AMD complex	38	54	28	5	18	32	36	30
AMD complex	29	43	29	3	40	45	18	30
	base pair rise (Å)							
	G1-A2	A2-A3	A3-G4	G4-C5	C5-T6	T6-T7	T7-C8	mean[b]
N8AMD complex	3.6	3.8	2.8	7.1	4.2	3.2	2.6	3.4
AMD complex	3.3	3.5	3.7	6.9	3.7	2.6	3.4	3.4

[a] The helix twist angles and base pair rise parameters are defined and calculated by the procedures recommended at the EMBO Workshop on DNA Curvature and Binding held at Churchill College in 1988. [b] The mean values calculated by excluding the rise at the intercalation site (G4-C5).

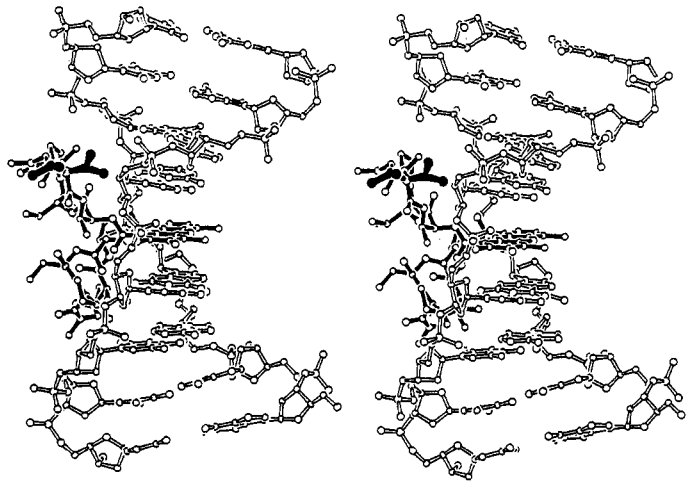

FIGURE 8: View showing the large space between the *N*-methyl-L-valine residue in the β-ring of N8AMD and the DNA minor groove. An additional isopropyl group (thick solid bonds), which represents the D-MeVal side-chain, is attached to the Cα of *N*-methyl-L-valine in order to show the probable effect of *N*-methyl-D-valine substitution. The isopropyl groups of *N*-methyl-L-valine and *N*-methyl-D-valine residues, drawn by thick solid bonds with filled circles, are placed at left and right of the Cα atom, respectively.

intercalation of a flat aromatic molecule, and the backbone of DNA is bent by the unwinding as observed in DNA strand-1. This bent conformation of the DNA backbone is apparently stabilized by forming a hydrogen bond between the amino group (N2) and O5′ of the C5 residue. As a result, the minor groove of the α-ring side creates a suitable pocket for the α-ring. Thus, the α-ring of the cyclic depsipeptide fits well into the minor groove without changing the conformation, as observed with AMD itself (Ginell *et al.*, 1988), and it apparently has favorable hydrophobic interactions with the minor groove surface. On the other hand, the negatively charged phosphate group in DNA strand-2 cannot come close to the negatively charged N8 atom and also cannot form any hydrogen bonds with the drug. Therefore, the DNA backbone lies away from the N8 atom (Figure 5). As a result, the structure of the minor groove on the β-ring side is somehow distorted. In contrast to the α-ring, the β-ring does not fit well into the minor groove; the proline residue in particular appears to be forced out of the minor groove. Thus, formation of a hydrogen bond between the amino group (N2) attached to the phenoxazone ring and the DNA backbone appears to break the 2-fold symmetry of the intercalation site, and the N8AMD molecule interacts with the DNA in an asymmetrical mode. As a result, the conformations of the two cyclic depsipeptides become quite different from each other. The exact same trends are observed in the backbone conformations of the two DNA strands and the ring conformations of the cyclic depsipeptides in the AMD complex (Figures 5 and 6). The sequence specificity of AMD, such as 5′-TGCA-3′ > 5′-AGCT-3′ reported by Chen (1992), might be due to the asymmetric binding mode of AMD.

As shown in Figure 8, there is a large space between the minor-groove surface and the *N*-methyl-L-valine residues in the β-ring. In addition, the hydrophobic isopropyl group of the *N*-methyl-L-valine residue points away from the DNA minor groove. Thus, if the *N*-methyl-L-valine is replaced with *N*-methyl-D-valine, the isopropyl group of *N*-methyl-D-valine should fit into the minor groove. If isopropyl group of the *N*-methyl-D-valine has favorable hydrophobic interactions with the deoxyribose ring of the DNA backbone, this analogue should bind strongly to DNA. To test this hypothesis, as well as the reliability of the structure determined by the 3.0 Å resolution data, the association constant of the *N*-methyl-D-valine-AMD (D-MeVal-AMD) analogue, which is a by-product of N8AMD (Chu *et al.*, 1994a), was determined and compared with those of N8AMD and AMD.

DNA Binding Characteristics of N8AMD, AMD, and D-MeVal-AMD. The binding characteristics of N8AMD, AMD, and D-MeVal-AMD were determined by measuring the visible absorption spectra. The spectra titrated with d(GAAGCTTC)$_2$ are shown in Figure 9, while the association constants calculated from the spectra, using the method developed in our laboratory, are listed in Table 5 (Chu *et al.*, 1994b). Although the crystal structure of N8AMD complexed with d(GAAGCTTC)$_2$ is quite similar to that of AMD, the association constant of N8AMD with the same DNA is much weaker than that of AMD. A similar difference between N8AMD and AMD was observed in the association constants with the non-self-complementary DNA (Chu *et al.*, 1994a). The weaker association constant of N8AMD is consistent with the fact that the N8AMD molecule can form an additional hydrogen bond with a water molecule (N8••H−O−H) in aqueous solution, which is not available to AMD. This hydrogen bonding probably stabilizes the N8AMD molecule in solution and tends to prevent its intercalation into the nucleic acid. As a result, the association constant of N8AMD is less than that of AMD.

As described above, the structure of the DNA−N8AMD complex suggested that substitution of the *N*-methyl-L-valine residue in the cyclic depsipeptide with a *N*-methyl-D-valine residue might increase the hydrophobic interaction with the minor groove of the DNA. In fact, the association constant of D-MeVal-AMD is higher than that of AMD. This indicates also that the structure of the d(GAAGCTTC)$_2$−N8AMD has been determined precisely enough to provide useful information in terms of DNA binding drug design.

RNA Polymerase Inhibitory Activities of N8AMD, AMD, and D-MeVal-AMD. The RNA polymerase inhibitory activities of N8AMD, AMD, and D-MeVal-AMD *in vivo* have been examined using human cells (HeLa). The drug concentrations at 50% inhibition level (IC_{50}) are listed in Table 5 along with the DNA association constants. The DNA association constants and the IC_{50} values are well correlated, indicating that the tighter the agent binds DNA,

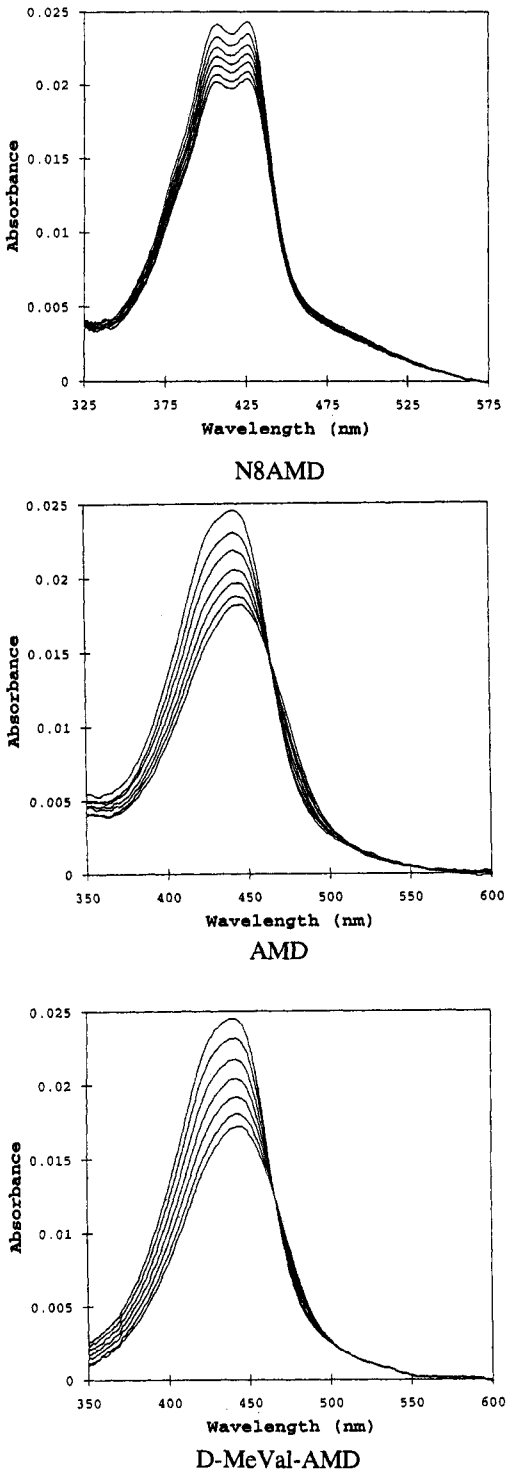

FIGURE 9: Visible absorption spectra of N8AMD, AMD, and D-MeVal-AMD titrated with d(GAAGCTTC)$_2$. The drug concentration is scaled to 1.0 μM. The ratios of [DNA]/[drug] are 0.0, 0.2, 0.4, 0.6, 0.8, 1.0, and 1.2 for N8AMD, 0.0, 0.15, 0.30, 0.45, 0.60, 0.75, and 0.90 for AMD, and 0.0, 0.12, 0.24, 0.36, 0.48, 0.60, and 0.72 for D-MeVal-AMD. The spectra of the drugs and each DNA titration are drawn from top to bottom, respectively.

the better it inhibits transcription activity. Although the DNA binding mode of N8AMD is quite similar to that of AMD in the crystal, the RNA synthesis inhibitory activity is substantially reduced. The D-MeVal-AMD analogue inhibits RNA synthesis more than AMD does, which is at least qualitatively consistent with the DNA binding behavior of this analogue.

Table 5: Association Constants (K M^{-1}) of N8AMD, AMD, and d-MeVal-AMD to d(GAAGCTTC)$_2$ and the Drug Concentrations (M) at 50% Inhibition of the RNA Synthesis (IC_{50}) in HeLa Cells

drug	K	IC_{50}
N8AMD	$3.3(5) \times 10^4$	$>1 \times 10^{-5}$
AMD	$1.1(1) \times 10^6$	3.5×10^{-8}
D-MeVal-AMD	$2.4(4) \times 10^6$	1.5×10^{-9}

ACKNOWLEDGMENT

We thank Mrs. Li Wen for DNA synthesis and Mrs. Judy Bevan for technical help with the transcription inhibition experiments. The Kansas Health Foundation is an independent, nonprofit organization whose mission is to improve the quality of health in Kansas.

REFERENCES

Brünger, A. T. (1993) *X-PLOR 3.1. A System for X-ray Crystallography and NMR*, Yale University Press, New Haven and London.
Cantor, C. R., & Warshaw, M. M. (1970) *Biopolymer 9*, 1059–1077.
Champoux, J. J., Gilboa, E., & Baltimore, D. (1984) *J. Virol. 49*, 686–691.
Chen, F.-M. (1988) *Biochemistry 27*, 6393–6397.
Chen, F.-M. (1992) *Biochemistry 31*, 6223–6228.
Chomczynski, P., & Sacchi, N. (1987) *Anal. Biochem. 162*, 156.
Chu, W., Kamitori, S., Shinomiya, M., Carlson, R. G., & Takusagawa, F. (1994a) *J. Am. Chem. Soc. 116*, 2243–2253.
Chu, W., Shinomiya, M., Kamitori, K., Kamitori, S., Carlson, R. G., Weaver, R. F., & Takusagawa, F. (1994b) *J. Am. Chem. Soc. 116*, 7971–7982.
Cirilli, M., Bachechi, F. , Ughetto, G., Colonna, F. P., & Capolianco, M. L. (1992) *J. Mol. Biol. 230*, 878–889.
Dickerson, R. E. (1989) *Nucleic Acids Res. 17*, 1797–1803.
Dickerson, R. E. (1992) *Methods Enzymol. 211*, 67–110.
Egli, M., Williams, L. D., Frederick, C. A., & Rich, A. (1991) *Biochemistry 30*, 1364–1372.
EMBO J. (1989) *8*, 1–4.
Frederick, C. A., Williams, L. D., Ughetto, G., van der Marel, G. A., van Boom, J. H., Rich, A., & Wang, A. H.-J. (1990) *Biochemistry 29*, 2538–2549.
Gao, Y.-G., Liaw, Y.-C., Robinson, H., & Wang, A. H.-J. (1990) *Biochemistry 29*, 10307–10316.
Gao, Q., Williams, D., Egli, M., Rabinovich, D., Chen, S.-L, Quigley, G. J., & Rich, A. (1991) *Proc. Natl. Acad. Sci. U.S.A. 88*, 2422–2426.
Gerard, G. F. (1981) *Biochemistry 20*, 256–264.
Ginell, S., Lessinger, L., & Berman, H. M. (1988) *Bipolymers 27*, 843–864.
Grula, M. A., & Weaver, R. F. (1981) *Insect Biochem. 11*, 149–154.
Jones, T. A. (1985) *Methods Enzymol. 115*, 157–171.
Kamitori, S., & Takusagawa, F. (1992) *J. Mol. Biol. 225*, 445–456.
Kamitori, S., & Takusagawa, F. (1994) *J. Am. Chem. Soc. 116*, 4154–4165.
Liaw, Y.-C., Gao, Y.-G., Robinson, H., van der Marel, G. A., van Boom, J. H., & Wang, A. H.-J. (1989) *Biochemistry 28*, 9913–9918.
Lipscomb, L. A., Peek, M. E., Zhou, F. X., Bertrend, J. A., VanDever, D., & Williams, L. D. (1994) *Biochemistry 33*, 3649–3659.
Matthews, B. W. (1968) *J. Mol. Biol. 33*, 491–497.
Moore, M. H., Hunter, W. N., d'Estaintot, B. L., & Kennard, O. (1989) *J. Mol. Biol. 206*, 693–705.
Nunn, C. M., Meervelt, L. V., Zhang, S., Moore, M. H., & Kennard, O. (1991) *J. Mol. Biol. 222*, 167–177.
Omer, C. A., & Faras, A. J. (1982) *Cell 30*, 797–805.
Quigley, G. J., Wang, A. H.-J., Ughetto, G., van der Marel, G. A., van Boom, J. H., & Rich, A. (1980) *Proc. Natl. Acad. Sci. U.S.A. 77*, 7204–7208.

Quigley, G. J., Ughetto, G. A., van der Marel, G. A., van Boom, J. H., Wang, A. H.-J., & Rich, A. (1986) *Science 232*, 1255−1258.

Resnick, R., Omer, C. A., & Faras, A. J. (1984) *J. Virol. 51*, 813−821.

Scamrov, A. V., & Beabealashvilli, R. Sh. (1983) *FEBS Lett. 164*, 97−101.

Sobell, H. M., & Jain, S. C. (1972) *J. Mol. Biol. 68*, 21−34.

Swanstorm, R., Varmus, H. E., & Bishop, J. M. (1981) *J. Biol. Chem. 256*, 1115−1121.

Takusagawa, F. (1982) *CRLS: Constrained-Restrained Least-Squares*, Technical Report ICR-1982-0001-0002-0001, The Institute for Cancer Research, Philadelphia, PA.

Takusagawa, F. (1992) *J. Appl. Crystallogr. 25*, 26−30.

Tanaka, I., Yao, M., Suzuki, M., Hikichi, K., Matsumoto, T., Kozasa, M., & Katayama, C. (1990) *J. Appl. Crystallogr. 23*, 334−339.

Ughetto, G., Wang, A. H.-J., Quigley, G. J., van der Marel, G. A., van Boom, J. H., & Rich, A. (1985) *Nucleic Acids Res. 13*, 2305−2323.

Verma, I. M. (1977) *Biochim. Biophys. Acta 473*, 1−38.

Wain-Holson, S., Sonigo, P., Danos, O., Cole, S., & Alizon, M. (1985) *Cell 40*, 9−17.

Wang, A. H.-J., Ughetto, G., Quigley, G. J., Hakoshima, T., van der Marel, G. A., van Boom, J. H., & Rich, A. (1984) *Science 225*, 1115−1121.

Wang, A. H.-J., Ughetto, G., Quigley, G. J., & Rich, A. (1986) *J. Biomol. Struct. Dyn. 3*, 319−342.

Wang, A. H.-J., Ughetto, G., Quigley, G. J., & Rich, A. (1987) *Biochemistry 26*, 1152−1163.

Williams, L. D., Egli, M., Gao, Q., Bash, P., van der Marel, G. A., van Boom, J. H., Rich, A., & Frederick, C. A. (1990a) *Proc. Natl. Acad. Sci. U.S.A. 87*, 2225−2229.

Williams, L. D., Egli, M., Ughetto, G., van der Marel, G. A., van Boom, J. H., Quigley, G. J., Wang, A. H.-J., Rich, A., & Frederick, C. A. (1990b) *J. Mol. Biol. 215*, 313−320.

BI950107C